ELSEVIER

Nuclear Physics A 587 (1995) 291–300

NUCLEAR PHYSICS A

Proton scattering by ^{8}He and neutron halo effects

L.V. Chulkov [a], C.A. Bertulani [b], A.A. Korsheninnikov [a]

[a] *Kurchatov Institute, Moscow 123182, Russia*

[b] *Universidade Federal do Rio de Janeiro, 21945-970 Rio de Janeiro, Brazil*

Received 14 November 1994; revised 28 December 1994

Abstract

The existing experimental data on ^{8}He+p elastic and inelastic scattering at low and high energies have been analyzed in terms of an eikonal approach with different presentations of nuclear density distributions. Comparison of calculations with experimental data reveals a sensitivity of recoil proton angular distribution at large momentum transfer to the shape of matter distribution. The root-mean-square radius of ^{8}He has been deduced and effects of neutron halo in ^{8}He are discussed.

1. Introduction

The development of new techniques for secondary radioactive beams has enabled unique experiments with exotic nuclei. It has been found that many peculiarities of neutron rich nuclei with low neutron binding energy can be explained in terms of the existence of a halo – a spatially prolonged distribution of the valence neutrons, extending far beyond a well defined core nucleus. In recent years many other properties of neutron-rich nuclei have attracted attention of many experimentalists and theorists as well.

The bulk of the experimental data has been obtained via the study of fragmentation reactions. Parameters of density distributions of halo nuclei have been derived by using Glauber type calculations (see Refs. [1,2], for example). These calculations might be insensitive to the shape of density distributions and might have mainly sensitivity to the root-mean-square (r.m.s.) nuclear radius [3]. However the comparison of the data obtained at different beam energies may reveal some dependence upon the density distributions [2].

Recently, experimental data on elastic scattering of very neutron rich nuclei became available [4–9]. Theoretical studies of elastic scattering of neutron rich nuclei have been done by several authors, e.g., in Refs. [10–16]. The experimental data on proton elastic

SSDI 0375-9474(95)00014-3

scattering [7–9] seem to give more unambiguous information due to the reaction mechanism simplicity. Despite these expectations, the calculations on halo nuclei scattering on protons [13–16] give rather contradictory information on the sensitivity to the halo appearance.

The aim of this article is to analyze in the parameter free eikonal approximation the existing experimental data on ^{8}He + p elastic and inelastic scattering at low [8] and high [9] energies for different models of nuclear matter distributions. The applicability of the eikonal approximation in the low energy region have been already discussed (Ref. [17], for example).

2. Elastic scattering in eikonal approximation

We describe briefly in this section the pertinent formulae used in elastic scattering calculations with the eikonal approximation.

We ignore spin–orbit effects and write the following expression [18] for the elastic scattering amplitude $f(\theta)$:

$$f(\theta) = -ik \int_0^\infty J_0(qb) \left[e^{i\chi(b)} - 1\right] db, \tag{1}$$

where k is the relative momentum, J_0 is the Bessel function of zero order, b is the impact parameter and q is the momentum transfer. The phase $\chi(b)$ contains nuclear and Coulomb parts, $\chi(b) = \chi_{\mathrm{nuc}}(b) + \chi_{\mathrm{Coul}}(b)$, where

$$\chi_{\mathrm{nuc}}(b) = -\frac{1}{\hbar w} \int_0^\infty U_{\mathrm{nuc}}(\sqrt{b^2 + z^2})\, dz, \tag{2}$$

$$\chi_{\mathrm{Coul}}(b) = \frac{2Z_1 Z_2 e^2}{\hbar w} \ln kb.$$

Next we construct the p+A optical potential using the "$t\rho$" approximation [22]. In this approximation the nucleon–nucleus optical potential is given by

$$U_{\mathrm{nuc}}(r) = \langle t_{\mathrm{pn}} \rangle \rho_{\mathrm{n}}(r) + \langle t_{\mathrm{pp}} \rangle \rho_{\mathrm{p}}(r), \tag{3}$$

$$\langle t_{\mathrm{p}N} \rangle = -\tfrac{1}{2} \hbar w \bar{\sigma}_{\mathrm{p}N} (\alpha_{\mathrm{p}N} + i),$$

where N = p or n and $\rho_N(r)$ is the neutron or proton density. The Pauli blocking corrected nucleon–nucleon total cross-section is given by [22]:

$$\bar{\sigma}_{\mathrm{p}N} = \sigma_{\mathrm{p}N}(E)(1 - \tfrac{7}{5} E_{\mathrm{F}}/E), \tag{4}$$

where E is the laboratory energy of the protons and $E_{\mathrm{F}} = \hbar^2 [3\rho_N(r)]^{2/3}/2m_N$ is the Fermi energy. The parameters $\sigma_{\mathrm{p}N}$ and $\alpha_{\mathrm{p}N}$ have been taken from Refs. [18,19] and are shown in Table 1.

Table 1
Parameters of an eikonal approximation

Energy [MeV/amu]	σ_{pp} [mb]	α_{pp}	σ_{pn} [mb]	α_{pn}
72	42.0	1.40	130	0.80
674	42.3	0.16	37.7	−0.35

It is worthwhile to mention that the approximation used for calculating the phase shift function, Eq. (2), is essentially the optical limit approximation. Generally speaking, this approximation might not be very accurate for those nuclei that have large density fluctuation, as in a halo structure (e.g., see Ref. [20]). However, a study performed in Ref. [21] shows that the optical limit approximation is fairy good for the angular region at least up to the second diffractive maximum even for the scattering on nuclei with well developed neutron halo structure.

3. The ^{8}He density distributions

We discuss next the following four parametrization of the ^{8}He density distributions.

COSMA: In the frame of the cluster-orbital shell-model approximation (COSMA) [23] the wave function for the system $\alpha + 4$ valence neutrons is written assuming the p3/2 state for the relative motion of the α-core and every valence neutron. The only scale parameter of the model was fitted to reproduce the ^{8}He experimental r.m.s. matter radius, $R_{m.s.}(^8\text{He}) = 2.52$ fm [24]. A simplified parametrization of single particle densities [23] as a sum of two gaussians were used in the calculations. The calculated nucleon density distribution is presented by the solid curve in Fig. 1a, where we show also densities for other models. The solid curves in Figs. 1b and c show separately the densities for neutrons and protons. This model gives an extended neutron distribution in ^{8}He; e.g., the r.m.s. radii for protons and neutrons are different: $R_{m.s.}(\text{p}) = 1.69$ fm and $R_{m.s.}(\text{n}) = 2.75$ fm. For the valence neutrons the r.m.s. radius is $R_{m.s.}(\text{valence}) = 3.1$ fm.

DROP: In the droplet-model approach [25,26], Fermi distributions are used for protons and neutrons, which are characterized by the same diffuseness, $a = 0.55$ fm, and radii $r_p = 0.937$ fm and $r_n = 2.19$ fm. The corresponding r.m.s. matter radius of ^{8}He has a value of 2.54 fm, which is close to experimental one.

The droplet-model density distribution is shown in Fig. 1a by a dashed curve. Proton and neutron components are shown by dashed curves in Figs. 1b and c. This model gives also an extended neutron distribution ($R_{m.s.}(\text{p}) = 2.16$ fm and $R_{m.s.}(\text{n}) = 2.66$ fm), but it differs from the COSMA result.

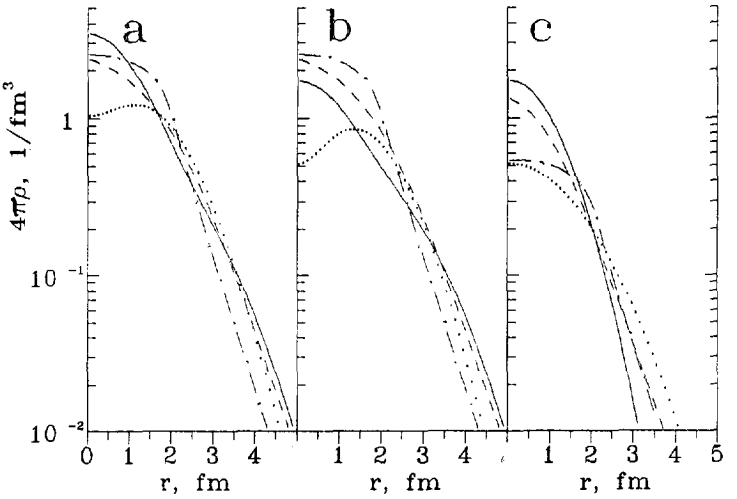

Fig. 1. Nucleon density distributions of ^{8}He. The result from COSMA is shown by a solid line, from DROP by a dashed line, from SW by a dot–dashed line and from DIS by a dotted line. (a) Total density distributions. (b) Neutron distributions. (c) Proton distributions.

SW: This parametrization for the density distribution was obtained by Sorensen and Winther [27]. The parametrization does not take into account the specific structure of ^{8}He and is not very realistic. In particular, the calculated r.m.s. matter radius (2.13 fm) differs from the experimental value (2.52 fm); the r.m.s. radii for protons and neutrons are almost equal ($R_{\mathrm{m.s.}}(\mathrm{p})$ = 2.17 fm, $R_{\mathrm{m.s.}}(\mathrm{n})$ = 2.12 fm) and does not correspond to the extended neutron distribution of ^{8}He. The calculated total density is shown by a dot–dashed curve in Fig. 1a, proton and neutron components are shown by dot–dashed curves in Figs. 1b and c.

DIS: The parameters of COSMA were modified to get the r.m.s radius of the neutron distribution almost equal to that of the proton, but keeping the same r.m.s. radius of ^{8}He. In this model the α-core is completely dissolved by the interaction with the valence neutrons and $R_{\mathrm{m.s.}}(\mathrm{n})$ = 2.52 fm equals to $R_{\mathrm{m.s.}}(\mathrm{p})$ = 2.52 fm, while $R_{\mathrm{m.s.}}(\mathrm{total})$ = 2.52 fm is equal to the experimental value of ^{8}He radius. The calculated densities are shown in Figs. 1(a,b,c) by dotted curves.

Now we use the four different models of ^{8}He density distributions for comparison. Three model densities (COSMA, DROP, DIS) have the same r.m.s. of ^{8}He radius. At the same time, these model densities differ one from another. Two of them (COSMA, DROP) yield a neutron tail extended beyond the α-core distribution while in the DIS model the neutron and proton distributions are similar. This is more evident in Figs. 1b and c where the proton and the neutron densities are presented separately. A comparison of the calculated angular distributions for these three models reveals the sensitivity to the different neutron and proton distributions while the comparison between other two models (SW and DIS) allows one to get a feeling of the sensitivity to nuclear

Table 2
Density distributions

Model	R_t [fm]	σ_t [fm]	R_n [fm]	σ_n [fm]	R_p [fm]	σ_p [fm]	$R_n - R_p$ [fm]
COSMA	2.52	1.10	2.75	1.11	1.69	0.66	1.06
DROP	2.54	0.85	2.65	1.02	2.16	0.96	0.49
SW	2.13	1.03	2.12	0.85	2.17	0.83	−0.05
DIS	2.52	0.89	2.52	0.85	2.52	0.98	0.00

radius. Unlike the COSMA density, which has a *good* α-core, the SW and DIS-models correspond to a strongly *melted* α-particle in ^{8}He (the valence neutrons penetrate into the α). The drop-model shows a less mixed α-core. Unlike Ref. [15], we shall not separate into two parts the neutron distribution – the core neutrons and the valence neutrons. Therefore effects of the nucleon–nucleon correlations are not account for.

The parameters of the different density distributions, namely, the r.m.s. values of radii, dispersions ($\sigma_N = \sqrt{\langle R_N^2 \rangle - \langle R_N \rangle^2}$), and differences in neutron and proton radii are summarized in Table 2.

4. Elastic ^{8}He + p scattering

The first experimental data on scattering of ^{8}He on protons have been obtained in RIKEN [8]. These are the data for elastic scattering (shown in Fig. 2 together with

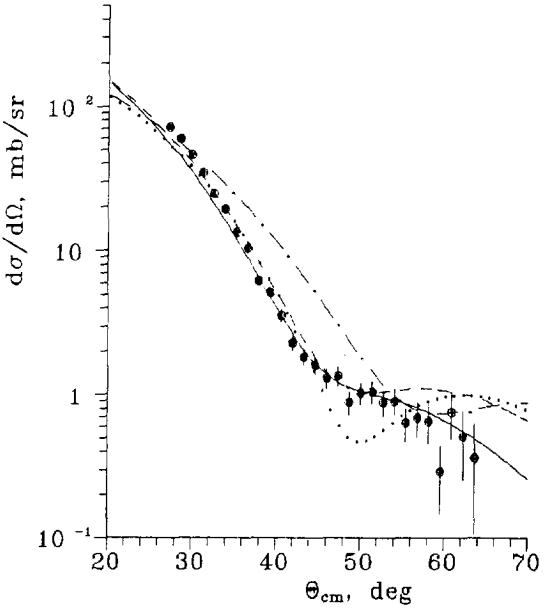

Fig. 2. The ^{8}He + p elastic scattering angular distribution at 72 MeV/nucleon. The experimental data were taken from Ref. [8]. Notations for different models are the same as in Fig. 1.

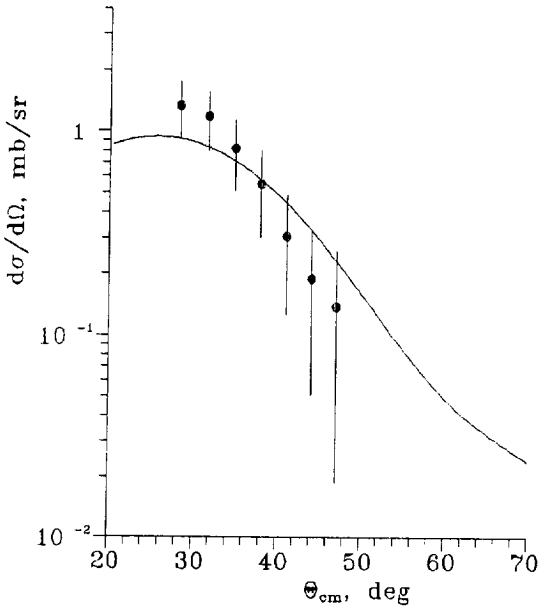

Fig. 3. The ^{8}He + p inelastic scattering angular distribution at 72 MeV/nucleon. The experimental data were taken from Ref. [8]. The solid line is the COSMA calculation.

experimental errors) as well as for inelastic scattering on the first excited state of ^{8}He (shown in Fig. 3). The analysis of the data has been done in Ref. [16] where the sensitivity of elastic scattering to the real part of potential has been studied. The elastic cross-section for this energy reveals refractive effects but the imaginary part of the $t\rho$ optical potential is quite deep. This favors a situation of a low sensitivity to the real part of potential. The method described here allows one to take into account the influence of the nuclear density distribution on the imaginary as well as on the real parts of the potential.

The calculations of ^{8}He elastic scattering with the four different density distributions are compared with the experimental data in Fig. 2. The three models with equal r.m.s. nuclear radii gave similar distributions (COSMA: solid line, DROP: dashed line, DIS: dotted line) with the position of the minimum at $\approx 50°$. The decreasing of the ^{8}He radius by 0.4 fm (SW) results in a shift to a large angles of the position of the diffractive minimum by about 8°. In this way we can derive the ^{8}He radius within an accuracy of

Table 3
Positions of the diffractive minima

R_t [fm]	R_n [fm]	θ_{cm} [72 MeV/nucleon]	R_p [fm]	θ_{cm} [674 MeV/nucleon]
2.52	2.75	49.3°	1.69	28.2°
2.54	2.65	49.7°	2.16	20.8°
2.13	2.12	58.1°	2.17	22.0°
2.52	2.52	50.0°	2.52	18.4°

≈ 0.1 fm. The ^{8}He r.m.s. radius deduced from elastic scattering is in good agreement with that derived from fragmentation experiments [24].

At the same time a weak dependence on the shape on matter distribution have been noticed. The COSMA and DROP calculations reproduce reasonably well the experimental data and differ only at large angles where experimental data have also large uncertainty. The DIS calculations yield a cross-section close to the minimum which is about 50% less than in the COSMA and DROP. It gives an evidence that models with neutron halo correspond to a better description of the experimental data. But one should notice that the cross-section close to the minima is also sensitive to many other effects, i.e., spin–orbit interactions, nucleon–nucleon correlations, etc. Therefore, the value of the cross-sections at this region is not so easily related to halo properties. An elastic scattering experiment at high energy may illuminate these ambiguities.

It is worthwhile to note here that at this energy the σ_{pn} is more than a factor of three higher than σ_{pp}. Besides, one has three times more neutrons than protons and the main features of the elastic scattering are determined by the neutron distribution. This can be seen in Table 3 where correlations between the nuclear as well as neutron radii and position of the diffractive minima are shown.

The sensitivity to the r.m.s. matter radius but not to the shape of matter distribution has also been obtained in our calculations for the inelastic scattering in the region where experimental data exist. The experimental data can be reproduced with the density distributions corresponding to a r.m.s. nuclear radius equal to 2.52 fm and a reasonable value of the deformation parameter, namely $\beta_2 = 0.3$. We consider the first excited state of the ^{8}He as a 2^+ state. The comparison of the COSMA model calculations with the experimental data are shown in Fig. 3. The formalism based on the eikonal approximation described in Ref. [28] was used in our calculations of the inelastic scattering.

The data for energies of more than several hundred MeV/nucleon are normally presented in a Lorentz invariant form. The angular distributions are given as a dependence of the $d\sigma/dt$ upon t, where t is a Mandelstam variable which has the meaning of momentum transfer. The large neutron halo may reveal itself in the elastic scattering at low momentum transfers, as was pointed out in Ref. [15] because the nucleon collisions occur far away from the nuclear core. But it is not so obvious how good this reasoning might be.

Fig. 4 presents the elastic scattering cross-section calculations at the energy of 674 MeV/u in the region of momentum transfer lower than 0.05 $(\mathrm{GeV}/c)^2$ ($\theta_{cm} \approx 10°$) in comparison with experimental data [9]. The weak dependence on the shape of density distributions and even upon the total radius is clearly seen from the picture. The calculations also show low sensitivity to the value of nucleon–nucleon cross-section as well as to the value of the α_{NN}-parameter. Thus, high precision experimental data are required to get information on the nucleus structure. The results for the models with neutron skin (COSMA,DROP) in momentum transfer region of 0.005–0.02 $(\mathrm{GeV}/c)^2$ reproduce satisfactorily experimental data but deviations of the other models do not exceed 15%.

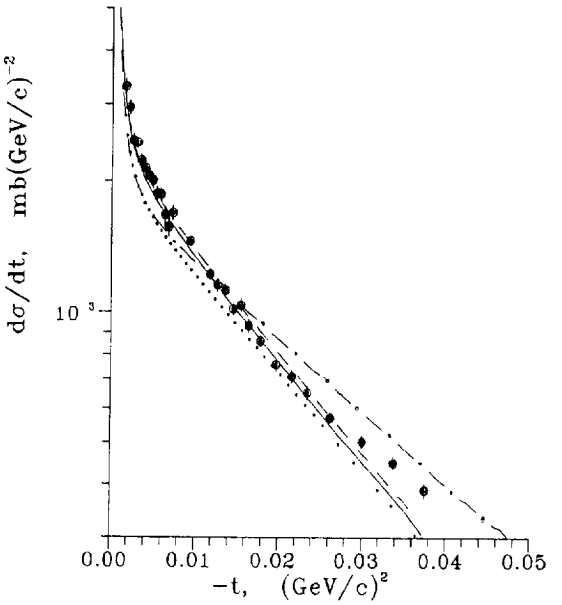

Fig. 4. The ^{8}He + p elastic scattering angular distribution at 674 MeV/nucleon in the low momentum transfer region. Very preliminary experimental data were taken from Ref. [9]. Notations for different models are the same as in Fig. 1.

At the same time, the elastic scattering cross-sections for the different models of ^{8}He differ drastically in the region of the diffractive minimum, as one can see in Fig. 5 where the calculations with the different ^{8}He models are shown. The position of the diffractive minimum is now very sensitive to the shape of density distribution and nicely correlated with the proton radii (see Table 3).

The cross-sections close to the minimum are also very sensitive to the difference in the proton and neutron distributions. The refraction effects are not very strong for this energy but they influence the cross-section close to the diffractive minimum. At a beam energy of about 500 MeV/nucleon the parameter α_{pp} becomes negative, while α_{pn} still remains positive. The real part of the optical model potential is then very sensitive to the difference between the neutron and the proton distributions because of the opposite sign of the contributions from the proton–neutron and proton–proton scattering amplitudes. The real part of the potential becomes repulsive and differs strongly in the region of maximal sensitivity for different density distributions. The small repulsive interaction results in a suppression of the cross-sections in the region of the minimum. But the cross-section in this region is also sensitive to the effects of nucleon–nucleon correlations [15], and possibly to some others effects, as we discussed before.

We conclude that the main information is contained in the position of the diffractive minimum. This dependence of this position upon the bombarding energy is a good tool to scan the density distribution of ^{8}He and allows one to reconstruct the nucleus structure.

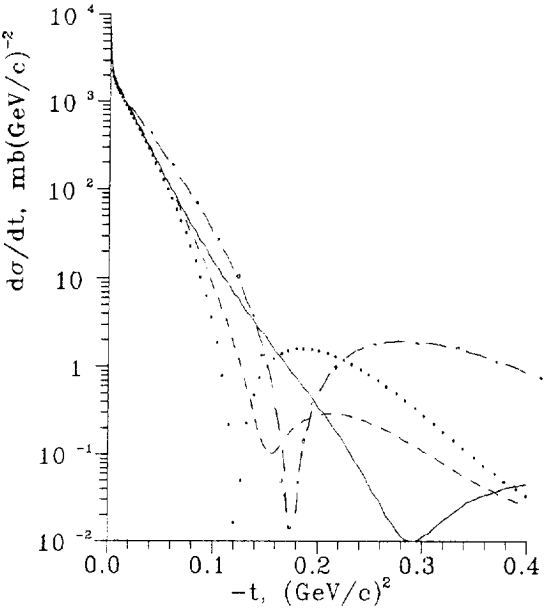

Fig. 5. The ^{8}He + p elastic scattering angular distribution at 674 MeV/nucleon. Notations for different models are the same as in Fig. 1.

5. Summary

We analysed the existing experimental data on ^{8}He + p elastic and inelastic scattering at low and high energies in terms of the eikonal approach with different presentations of nuclear density distributions. The analysis allowed us to get a definite value of the r.m.s. radius of ^{8}He which was found to be in a good agreement with that obtained from a fragmentation experiment [24]. The models of ^{8}He with neutron skin yield the better reproduction of experimental data. But the sensitivity to the shape of matter distribution for the energy of 72 MeV/nucleon as well as in the region of small momentum transfer ($\leqslant 0.04$ (GeV/c)^{2}) for the energy of 674 MeV/nucleon is weak and does not allow to determine which of the nuclear models with the same r.m.s. radius is more appropriate.

At the same time, for high energies the position of the diffractive minimum drastically depends on the shape of the density distribution. That is why the elastic scattering may become a good tool to study the neutron and proton density distributions inside halo nuclei. The analyses of measurements in vicinity of the diffractive minimum at low (around 100 MeV/u) and high (500–700 MeV/u) energies may lead to self-consistent descriptions. This might yield precious information not only on the matter radii of nuclei but also on the proton and neutron distributions inside the halo nuclei. We emphasize, however, that the sizes of unstable nuclei extracted from simple Glauber-type calculations should be taken with some reservations (e.g., Ref. [3]). For a more extensive calculation for He isotopes, see, e.g., Refs. [29–31].

References

[1] Y. Suzuki, K. Yabana and Y. Ogawa, Phys. Rev. C 47 (1993) 1317.
[2] I. Tanihata, T. Kobayashi, T. Suzuki, K. Yoshida, S. Shimoura, K. Sugimoto, K. Matsuta, T. Minamisono, W. Christie, D. Olson and H. Wieman, Phys. Lett. B 287 (1992) 307.
[3] L.V. Chulkov, B.V. Danilin, V.D. Efros, A.A. Korsheninnikov and M.V. Zhukov, Europhys. Lett. 8 (1989) 245.
[4] R.J. Smith, J.J. Kolata, K. Lamkin, A. Morsad, F.D. Becchetti, J.A. Brown, W.Z. Liu, J.W. Janecke, D.A. Roberts and R.E. Warner, Phys. Rev. C 43 (1991) 2346.
[5] J.J. Kolata, M. Zahar, R. Smith, K. Lamkin, M. Belbot, R. Tighe, B.M. Sherrill, N.A. Orr, J.S. Winfield, J.A. Winger, S.J. Yennello, G.R. Satchler and A.H. Wuosmaa, Phys. Rev. Lett. 69 (1992) 2631.
[6] M. Lewitowicz, C. Borcea, F. Carstoiu, M.G. Saint-Laurent, A. Kordyasz, R. Anne, P. Roussel-Chomaz, R. Bimbot, V. Borrel, S. Dogny, D. Guillemaud-Mueller, A.C. Mueller, F. Pougheon, F.A. Gareev, S.N. Ershov, S. Lukyanov, Yu. Penionzhkevich, N. Skobelev, S. Tretyakova, Z. Dlouhy, L. Nosek and J. Svanda, Nucl. Phys. A 562 (1993) 301.
[7] C.-B. Moon, M. Fujimaki, S. Hirenzaki, N. Inabe, K. Katori, J.C. Kim, Y.K. Kim, T. Kobayashi, T. Kubo, H. Kumagai, S. Shimoura, T. Suzuki and I. Tanihata, Phys. Lett. B 297 (1992) 39;
C.-B. Moon, K. Abe, M. Fujimaki, N. Inabe, K. Katori, J.C. Kim, Y.K. Kim, T. Kobayashi, H. Kumagai, T. Kubo, S. Shimoura, T. Suzuki and I. Tanihata, preprint RIKEN-AF-NP-126 (1992).
[8] A.A. Korsheninnikov, K. Yoshida, D.V. Aleksandrov, N. Aoi, Y. Doki, N. Inabe, M. Fujimaki, T. Kobayashi, H. Kumagai, C.-B. Moon, E.Yu. Nikolsky, M.M. Obuti, A.A. Ogloblin, A. Ozawa, S. Shimoura, T. Suzuki, I. Tanihata, Y. Watanabe and M. Yanokura, Phys. Lett. B 316 (1993) 38.
[9] S. Neumaier, G.D. Alkhazov, N.M. Andronenko, T. Betha, K.-H. Behr, K. Burkard, A.V. Dobrovolski, P. Egelhof, C. Fisher, G.E. Gavrilov, H. Geissel, H. Inrich, A.V. Khanzadeev, G.A. Korolev, A.A. Lobodenko, P. Lorenzen, G. Münzenberg, M. Mutterer, F. Nickel, W. Shwab, D.M. Seliverstov, P. Singer, T. Suzuki, J.P. Theobald, N.A. Timofeev, A.A. Vorobyov and V.I. Iatsoura, preprint GSI-94-43 (1994).
[10] G.R. Satchler, K.W. McVoy and M.S. Hussein, Nucl. Phys. A 522 (1991) 621.
[11] A.N.F. Aleixo, C.A. Bertulani and M.S. Hussein, Phys. Rev. C 45 (1992) 2403.
[12] M.C. Mermaz, Phys. Rev. C 47 (1993) 2213.
[13] A.N.F. Aleixo, C.A. Bertulani and M.S. Hussein, Phys. Rev. C 43 (1991) 2722.
[14] S. Hirenzaki, H. Toki and I. Tanihata, Nucl. Phys. A 552 (1993) 57.
[15] G.D. Alkhazov and A.A. Lobodenko, Yad. Fiz. 56 (3) (1993) 89 [Phys. At. Nuclei 56 (1993) 337].
[16] S.A. Goncharov and A.A. Korsheninnikov, preprint RIKEN-AF-NP-163 (1993).
[17] I. Brissaud, L. Bimbot, Y. Le Bornec, B. Tatischeff and N. Willis, Phys. Rev. C 11 (1975) 1537.
[18] C.A. Bertulani, L.F. Canto and M.S. Hussein, Phys. Reports 226 (1993) 283.
[19] L. Ray, Phys. Rev. C 20 (1979) 1957.
[20] Y. Ogawa, K. Yabana and Y. Suzuki, Nucl. Phys. A 543 (1992) 722.
[21] N. Takigawa, M. Ueda, M. Kuratani and H. Sagawa, Phys. Lett. B 288 (1992) 244.
[22] M.S. Hussein, R.A. Rego and C.A. Bertulani, Phys. Reports 201 (1991) 279.
[23] M.V. Zhukov, A.A. Korsheninnikov and M.S. Smedberg, Phys. Rev. C 50 (1994) R1.
[24] I. Tanihata, Nucl. Phys. A 478 (1988) 795c.
[25] W.D. Myers, Nucl. Phys. A 204 (1973) 465.
[26] W.D. Myers and K.-H. Schmidt, Nucl. Phys. A 410 (1983) 61.
[27] J.H. Sorensen and A. Winther, Nucl. Phys. A 550 (1992) 329.
[28] C.A. Bertulani, Nucl. Phys. A 539 (1992) 163.
[29] B.V. Danilin, M.V. Zhukov, A.A. Korsheninnikov and L.V. Chulkov, Sov. J. Nucl. Phys. 53 (1991) 45.
[30] M.V. Zhukov, B.V. Danilin, D.V. Fedorov, J.M. Bang, I.J. Thompson and J.S. Vaagen, Phys. Reports 231 (1993) 151.
[31] K. Varga, Y. Suzuki and Y. Ohbayasi, Phys. Rev. C 50 (1994) 189.